Chapter 10
Distributed Solar-PV Generation: Impact on Voltage Control and Stability

Lasantha Meegahapola and Tim Littler

10.1 Introduction

Solar-PV generation has gained significant momentum over the past two decades as one of the most viable renewable power generation options and has contributed significantly to achieve sustainable energy targets in many power networks across the world. Consequently, electricity network operators have been required to solve various planning, operational, and control issues with the increasing penetration of distributed solar-PV generation [1, 2]. These issues include intermittency and volatility, voltage control and regulation, stability, and line congestion.

Unlike other renewable power generation technologies, the majority of solar-PV generators are connected to power distribution feeders. This paradigm shift has resulted in bidirectional power flow in distribution feeders, requiring utilities to manage potential voltage rise issues as solar-PV penetration levels increase [3]: in particular, voltage rise can affect consumer equipment protection and transformer lifetime. Therefore, distribution utilities must develop innovative methods to regulate distribution feeder voltage profile within stipulated limits defined by standards.

The preservation of voltage stability is one of the major challenges faced by the power network operators. Typically, synchronous generators provide a significant portion of network reactive power; however, as solar-PV penetration levels

L. Meegahapola (✉)
Electrical and Computer Engineering,
RMIT University, Melbourne 3000, Australia
e-mail: lasantha.meegahapola@rmit.edu.au

T. Littler
School of Electronics, Electrical Engineering & Computer Science,
the Queen's University Belfast, Co. Antrim,
BT9 5AH Belfast, Northern Ireland, UK
e-mail: t.littler@qub.ac.uk

R. Bansal (ed.), *Handbook of Distributed Generation*,
DOI 10.1007/978-3-319-51343-0_10

increase, conventional synchronous generating units are displaced. Subsequently, network reactive power levels decrease as solar-PV generators are not capable of providing sufficient reactive power to replace large-scale reactive power levels provided by synchronous units [1, 2]. Therefore, careful management of voltage stability is required to sustain higher penetration of solar-PV generation.

This chapter investigates the distribution feeder voltage control and voltage stability issues resulting from greater penetration of solar-PV generation in electricity networks. Voltage stability is investigated using static and dynamic methods. This chapter also critically evaluates various strategies that can be used for distribution feeder voltage regulation and voltage stability improvement in the context of high penetration of solar-PV generation.

10.2 Modelling of Solar-PV Systems

A solar-PV system is comprised of a number of different components: a solar-PV panel, DC-DC boost converter, voltage source inverter (VSI), inverter controller and maximum power point tracking (MPPT) system, and an LCL filter. It is essential to model each component of the solar-PV system in detail to accurately represent the behaviour of the solar-PV system for dynamic simulations. A discussion of the dynamic simulation model of the solar-PV system is based on an actual 5 kW single-phase solar-PV system. The schematic diagram of the dynamic simulation model for a single-phase solar-PV system is shown in Fig. 10.1.

The 5 kW solar-PV array is comprised of two parallel rows, and each row contains ten series-connected PV panels. The parameters of an actual solar-PV panel [4] are shown in Table 10.1.

Using the parameters in Table 10.1, and by following the methodology outlined in [5], I-V and P-V curves were produced for the 5 kW PV array. It is assumed that the solar-PV array is exposed to an ambient temperature of 25 °C (Fig. 10.2).

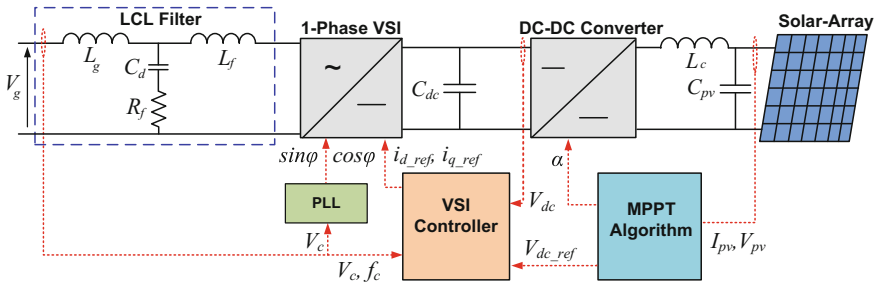

Fig. 10.1 Dynamic simulation model of a single-phase solar-PV system

Table 10.1 Solar-PV panel parameters

Parameter	Value
Nominal power—P_{MP} (Wp)	250
Nominal power voltage—V_{MPP} (V)	30.2
Nominal power current—I_{MPP} (A)	8.30
Open-circuit voltage—V_{OC} (V)	37.4
Short-circuit current—I_{SC} (A)	8.86
Module efficiency (%)	15.1
Temperature coefficient of P_{MPP} (%/°C)	−0.40
Temperature coefficient of V_{OC} (%/°C)	−0.27
Temperature coefficient of I_{SC} (%/°C)	0.024

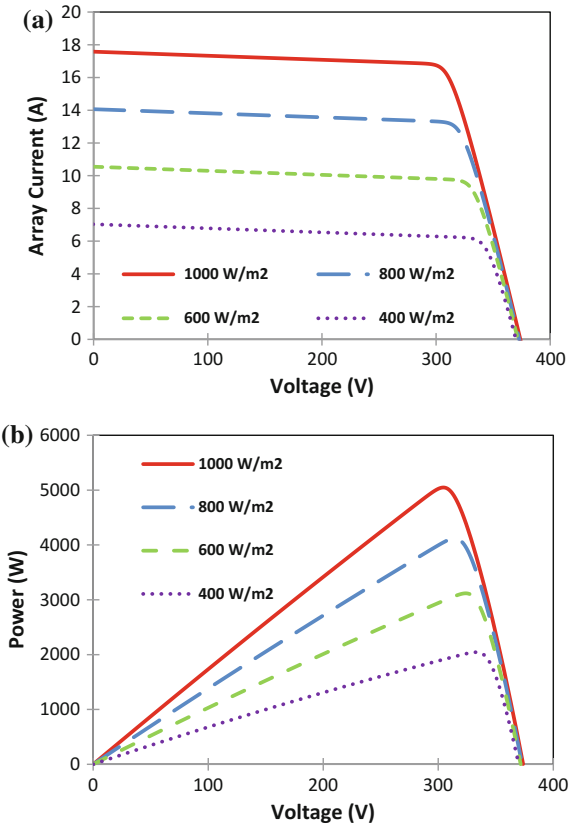

Fig. 10.2 5 kW solar-PV array's characteristics: **a** I-V curve and **b** P-V curve

The dynamic simulation model of the solar-PV system has the capability to respond variable solar irradiation and ambient temperature conditions. The MPPT system is based on the incremental conductance (IC) algorithm [6], since this algorithm performs well under rapid variations in solar irradiance. The VSI is rated

at 5.5 kVA and represented by an average converter model. The LCL filter parameters (L_g, C_d, L_f) are selected based on the methodology outlined in [7]. The DC link capacitor (C_d), input filter capacitor (C_{pv}), and DC coupling inductor (L_c) sizes were determined based on [8]. The solar-PV system was designed with the capability to control voltage at the point of common coupling (PCC) of solar-PV system. The solar-PV system active and reactive power control schemes are shown in Fig. 10.3.

Active power reference (P_{ref}) is determined by taking the difference between the actual (V_{dc}) and reference DC link (V_{dc_ref}) voltages, and then, by feeding the active power reference through a PI controller, the *d-axis* current reference (I_{d_ref}) is determined. A further control loop is established in the active power control loop in order to decrease active power generation during over-frequency events. The reactive power reference is determined by calculating the difference between the actual (V_{ac}) and reference (V_{ac_ref}) AC voltages at the solar-PV system PCC; then, the reactive power reference is feed through a PI controller to determine the *q-axis* current reference (I_{q_ref}). The current limiter *d-axis* current reference receives priority, while the *q-axis* current reference will be limited by the current rating of the inverter.

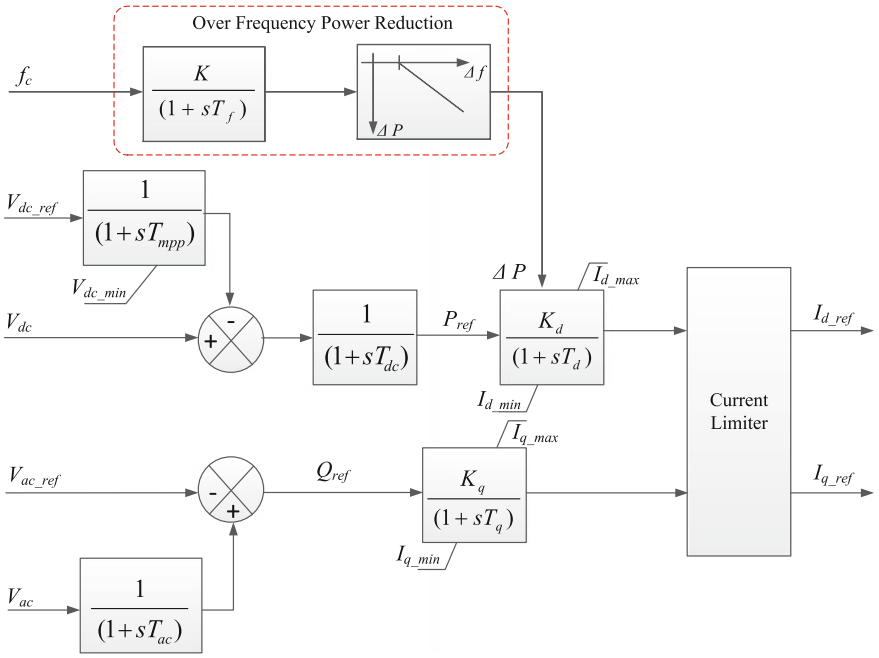

Fig. 10.3 Solar-PV model active and reactive power control scheme

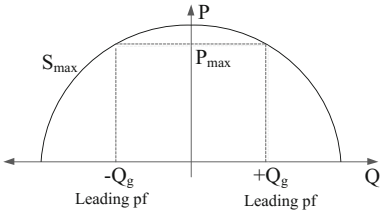

Fig. 10.4 Solar-PV system capability curve

10.2.1 Active and Reactive Power Characteristics

The active and reactive power characteristics of the solar-PV system depend on the rating of the inverter. Typical inverters are rated with 10% more than the active power rating; hence, they can still produce some reactive power at the full active power output. The active and reactive power characteristics of a typical solar-PV system are shown in Fig. 10.4.

10.3 Voltage Regulation in Distribution Feeders

In conventional power distribution feeders, power flow is unidirectional; hence, the voltage decreases from the LV side of the distribution transformer towards the end of the feeder. This voltage drop can be easily understood by considering a distribution feeder with a line impedance of $R + jX$ and upstream source V_s, as in Fig. 10.5.

A $P + jQ$ load is connected at the receiving end; hence, the sending-end voltage (V_s) can be approximated by:

$$\begin{aligned} V_s = V_r = (R+jX)I \quad \text{where } I = \frac{(P-jQ)}{V_r^*} \\ \Rightarrow V_s = \left[V_r + \frac{RP+XQ}{V_r}\right] + j\left[\frac{XP-PQ}{V_r}\right] \end{aligned} \tag{10.1}$$

The sending-end voltage given in (10.1) can be presented in the following form:

$$V_s = V_r + \Delta V_m + j\Delta V_p \tag{10.2}$$

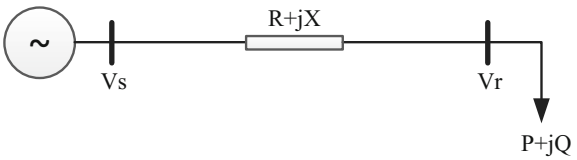

Fig. 10.5 LV distribution feeder model

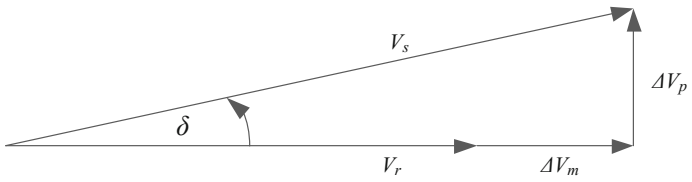

Fig. 10.6 Phasor diagram representation for voltage drop along a feeder

Magnitude change: $\Delta V_{\mathrm{p}} = \frac{XP-RQ}{V_{\mathrm{r}}}$ Phase change: $\Delta V_{\mathrm{m}} = \frac{RP+XQ}{V_{\mathrm{r}}}$.
This can be represented by a phasor diagram as follows (Fig. 10.6):
The phase angle δ is too small for distribution networks, and hence,

$$\Delta V_{\mathrm{p}} << V_{\mathrm{r}} + \Delta V_{\mathrm{m}} \tag{10.3}$$

Therefore, the sending-end voltage can be approximated as follows:

$$V_{\mathrm{s}} = V_{\mathrm{r}} + \frac{RP + XQ}{V_{\mathrm{r}}} \tag{10.4}$$

The voltage drop in the distribution feeder can be approximated as follows:

$$V_{\mathrm{s}} - V_{\mathrm{r}} = \Delta V = \frac{RP + XQ}{V_{\mathrm{r}}} \tag{10.5}$$

The voltage drop in the distribution feeder depends on the power factor of the connected load and the impedance of the distribution feeder. The voltage drop in a distribution feeder is typically treated as voltage regulation. Voltage regulation is strongly influenced by the load power factor and is largest for a lagging power factor and smallest—or even negative—for a leading power factor. Voltage regulation is defined as follows:

$$\begin{aligned} &\text{Voltage Regulation (VR)} = (V_{\mathrm{nl}} - V_{\mathrm{fl}})/V_{\mathrm{fl}} = (V_{\mathrm{s}} - V_{\mathrm{r}})/V_{\mathrm{r}} \\ &\Rightarrow \text{Voltage Regulation (VR)} = \frac{(RP + XQ)}{V_{\mathrm{r}}^2} \end{aligned} \tag{10.6}$$

where V_{fl} and V_{nl} are defined as voltage at full load and voltage at no load, respectively. When distribution feeder is considered, V_{fl} can be considered as voltage at the source, and V_{nl} can be considered as the voltage at the load end (receiving end).

Line losses are given by:

$$\begin{aligned} \text{Line Losses} = I^2R &= \left[\frac{(P - jQ)}{V_r^*}\right]^2 R \\ \Rightarrow \text{Line Losses} &= \left[\frac{(P^2 + Q^2)}{V_r^2}\right] R \end{aligned} \tag{10.7}$$

According to Eq. (10.7), both active and reactive power contribute to line losses, and hence, reactive power flow in the distribution line must be minimised in order to decrease the line losses.

Illustration *An 11* kV *15*-km *distribution feeder delivers power to a 150 kW load. The distribution feeder has a per-length impedance of 0.3 + j0.031 Ω/km. The load power factor is changed from 0.8 lagging to 0.8 leading while maintaining the receiving-end voltage at 11* kV. *The distribution feeder voltage drop and line losses are shown in* Fig. 10.7.

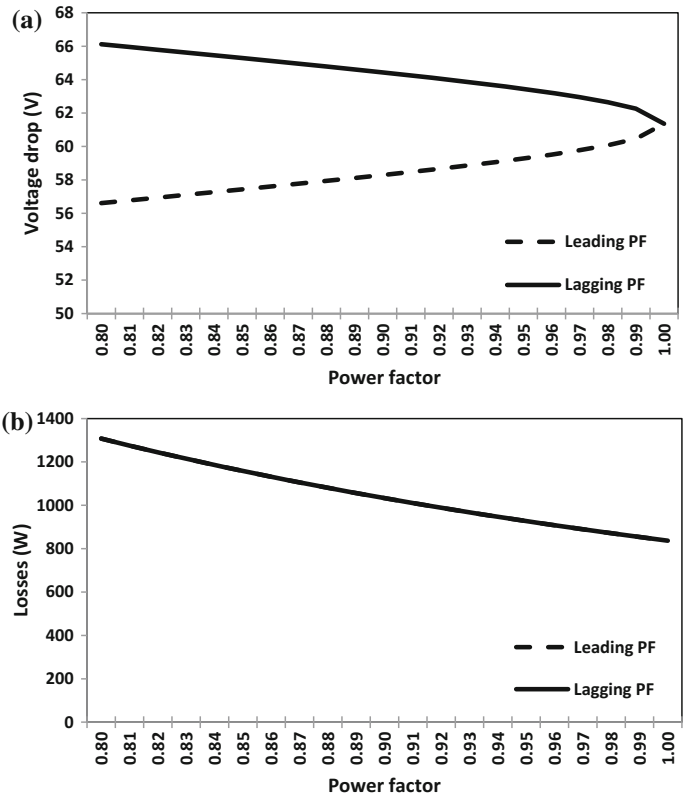

Fig. 10.7 Distribution feeder performance: **a** voltage drop variation with power factor and **b** line loss variation with power factor

According to Fig. 10.7a, when the leading power factor of the load is increased from 0.80 to 0.99, the voltage drop increased from 56.61 to 60.46 V. Conversely, a lagging power factor of the load increased from 0.80 to 0.99 and the voltage drop decreased from 66.12 to 62.26 V. However, irrespective of the load operating as either a leading or a lagging power factor, system losses are decreased with an improved load power factor. Therefore, a large reactive power has resulted in greater losses in the network.

10.3.1 Voltage Regulation Standards

Typically, utilities follow the voltage regulation standards stipulated by various standard bodies, such as IEC. The IEC 60038 is one of the commonly adopted standards in many countries for voltage regulation. The stipulated LV/MV voltage ranges in IEC 60038 are given in Table 10.2.

According to Table 10.2, the voltage regulation limits for different voltage levels are defined in three different time frames and peak impulse voltage is defined separately. The steady-state voltage is the main focus of this chapter; hence, according to the IEC 60038 for a residential distribution feeder, the allowable voltage range is 216.2–253 V. Typically, the voltage varies along the feeder based on the connected load; hence, distribution utilities apply various strategies to maintain the voltage within these limits.

10.3.2 Methods to Improve Distribution Feeder Voltage Regulation

Aforementioned, distribution utilities use various methods to regulate the feeder voltage profile and maintain the voltage within limits stipulated by standards. The following approaches are commonly used in distribution feeders to regulate the feeder voltage profile:

Table 10.2 Voltage standards specified in IEC 60038

Voltage level (kV)	Timescale			Peak impulse voltage (kV)
	Steady state	<1 min.	<10 s	
<1	+10% to −6%	+14% to −10%	+50% to 100% (L-E) +20% to 100% (L-L)	6
1 to 6.6	±6% (± 10% rural)	±10%	+80% to 100% (L-E) +20% to 100% (L-L)	60
11				95
22				150
66	±10%	±15%	+50% to 100% (L-E) +20% to 100% (L-L)	325

- Tap-changing transformers,
- Shunt capacitors and reactors,
- Line voltage regulators,
- Static VAr systems, and
- Static synchronous compensators (STATCOMs).

- Tap-Changing Transformers.

Tap-changing transformers can be divided into two types: (i) offload and (ii) on-load transformers. Typically, offload transformers are used in LV distribution feeders, while on-load units are used for primary distribution feeders. Offload transformers are typically *fixed tap*, and their tap settings are typically changed during summer and winter periods.

It is assumed that two tap-changing transformers are installed at both the sending- and receiving-end of the feeder as shown in Fig. 10.8.

Then, by considering a single-phase equivalent circuit of a radial distribution feeder with two tap-changing transformers (as shown in Fig. 10.8), the voltage drop of the feeder can be calculated as given in Eq. (10.8), [9],

$$\Delta V = V_1(t_s/t_r) - V_2 \approx \frac{RP + XQ}{t_r^2 V_2} \tag{10.8}$$

The product of t_r t_s is maintained at unity; this ensures that the overall voltage level remains in the same order.

In certain cases, voltage control of the transformer includes a measurement of current through the transformer. This is known as line-drop compensation (LDC) and allows the voltage to be controlled at a remote point of the distribution feeder, as shown in Fig. 10.9. The LDC is incorporated with the measured voltage as follows:

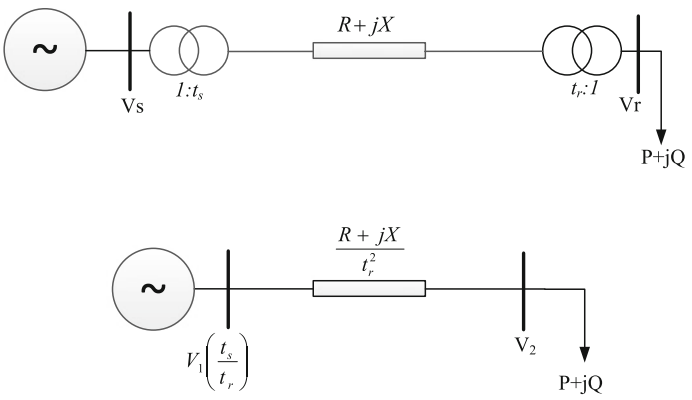

Fig. 10.8 Distribution feeder with tap-changing transformers

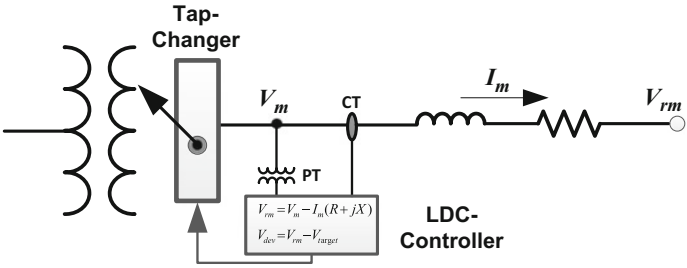

Fig. 10.9 Line-drop compensation (LDC) scheme of the transformer [10]

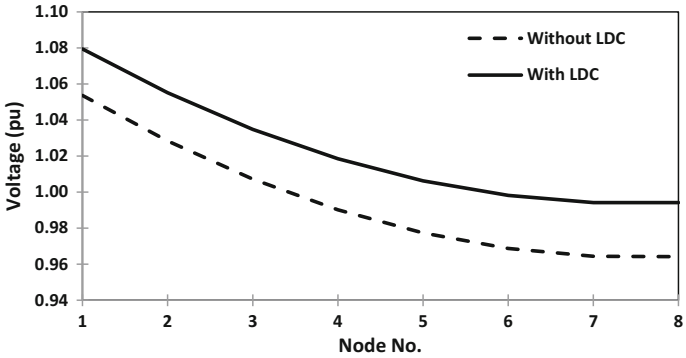

Fig. 10.10 Comparison of feeder voltage profile with and without LDC

$$V_{\mathrm{rm}} = V_{\mathrm{m}} - I_{\mathrm{m}}(R + jX)$$

$V_{\mathrm{dev}} = V_{\mathrm{rm}} - V_{\mathrm{target}}$ where V_{m}, I_{m}, and V_{rm} are the measured voltage, measured current, and effective voltage at the remote location of the feeder. Then, the voltage deviation (V_{dev}) from the target voltage (V_{target}) is calculated to determine the tap position.

Figure 10.10 illustrates the voltage profile of an MV distribution feeder with and without LDC.

It must be noted that transformer is located at the node 1, while the LDC is applied to control the voltage at node 8 to arrest the voltage at 1 pu (with a lower bound of 0.99 pu and an upper bound of 1.01 pu). According to Fig. 10.10, once the LDC is applied for node 8, transformer tap position is adjusted to arrest the node 8 voltage within the bounds despite the voltage rise at node 1.

- Shunt Capacitors and Reactors

Shunt capacitors are used to compensate lagging power factor loads, while the reactors are used for feeders which generate reactive power on lightly loaded

cables. Shunt capacitors are directly connected to the busbar and tertiary winding of transformers. In certain conditions, capacitors are installed along a distribution feeder to compensate for losses and any voltage drop. The reactive power dispatch from a capacitor or a reactor is given by:

$$Q = \frac{V^2}{X}, \quad X_c = \frac{1}{\omega C} \quad \text{or} \quad X_L = \omega L \tag{10.9}$$

The reactance X can be either capacitive (X_C) or inductive (X_L). However, if the voltage decreases, the reactive power produced by the shunt capacitors and reactors will decrease in proportion to the square of the voltage.

- Line Voltage Regulators

Voltage regulators are autotransformers with automatically adjusting taps. Commonly, regulators provide a range from –10 to + 10% with 32 steps. A single-phase regulator has three terminals: the source (S), the load (L), and the source–load (SL). The series winding is between S and L. The line current is measured at the load terminal (L) using a current transformer (CT), while the voltage is measured between the load (L) and source–load (SL) terminals using a potential transformer (PT). A regulator controller uses the measured current and voltage values to determine the required tap setting for regulation. Tap changing is normally performed by a relay mechanism with three settings: (i) *Set Voltage*—the desired output voltage of the regulator; (ii) *Bandwidth*—parameter used to initiate tap operation when the difference between the set voltage and measured voltage exceeds half of the bandwidth; and (iii) *Time Delay*—the waiting time between the time when the voltage goes out of band and when the controller initiates a tap [11]. If the voltage is still out of bounds after a tap change, the controller makes additional tap changes until the voltage is brought within bounds. A schematic diagram of the regulator windings is shown in Fig. 10.11.

- Static VAr Compensator (SVC) Systems

An SVC is a combination of thyristor-switched capacitor banks and thyristor-controlled inductors. SVCs are capable of delivering both capacitive and inductive reactive power based on the terminal voltage of the SVC. However, as the capacitors and inductors of the SVC are directly exposed to the terminal voltage, reactive power capability is affected by the magnitude of the terminal voltage. Therefore, an SVC performs well only when the terminal voltage is >0.9 pu, and its reactive power capability linearly decreases with reduction in terminal voltage [12]. Therefore, SVCs are not effective under large system contingencies, such as short-circuit faults as they fail to deliver adequate reactive power to compensate a voltage drop in the network.

- Static Synchronous Compensators (STATCOMs)

A STATCOM is comprised of a voltage source convertor (VSC), a capacitor, and a coupling transformer. If the terminal voltage magnitude is less than the preset

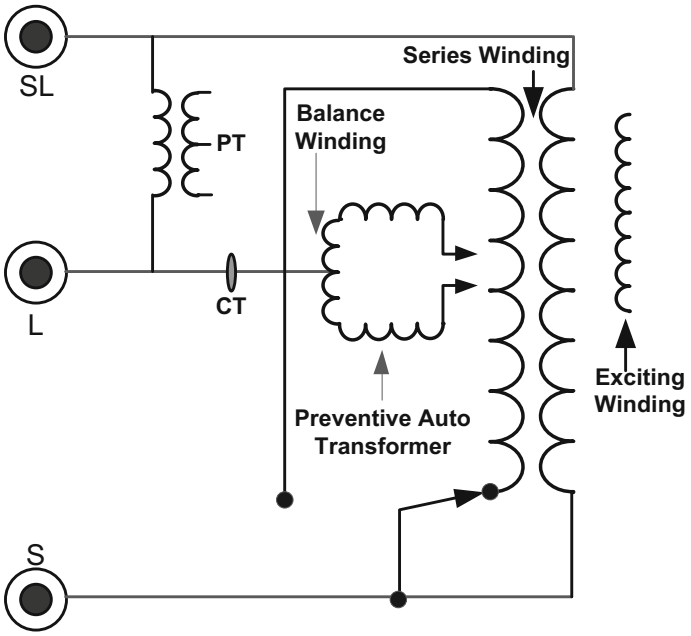

Fig. 10.11 Configuration of the line voltage regulator

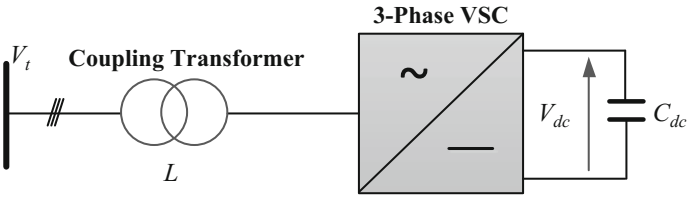

Fig. 10.12 A schematic of a STATCOM

voltage, then the STATCOM will generate capacitive reactive power, whereas if the terminal voltage is higher than the preset voltage, the STATCOM will render inductive reactive power. During normal operation, the STATCOM voltage lags the network voltage by a small angle in order to maintain capacitor charge. The main advantage of the STATCOM is its superior dynamic performance even at very low voltage levels [12]. Typically, a STATCOM is capable of delivering the rated capacitive reactive power even at very low voltage levels such as 0.2 pu (Fig. 10.12).

10.4 Impact of Solar-PV Generation on Feeder Voltage Regulation

Renewable power penetration has significantly increased during the last decade due to improvements in power electronic converter technologies and government directives to reduce greenhouse gas emissions (GHGs). The majority of renewable generation has been integrated at medium-voltage (MV) and low-voltage (LV) distribution feeders; generation sources of this type are commonly known as distributed generators (DGs). Conventional distribution networks are designed for power flow in one direction; however, with the integration of DGs, power flow is potentially bidirectional, resulting in variation (with possible violation) of voltage standards [13]. In particular, during high DG penetration levels, the upper voltage limit can be exceeded. The penetration level is defined as the ratio of power generated by the DG to the total connected load to the feeder, in percentage at any given time. If the penetration level is over 50%, then it could be considered as high penetration.

Consider the distribution feeder shown in Fig. 10.13, which contains a distributed generator connected at the load end of the feeder. The distributed generator generates $P_G + jQ_G$.

With the distributed generator installed at the end of the feeder, the voltage at the receiving end depends on the net power at the receiving-end busbar. Therefore, Eq. (10.4) can be modified based on the net power flow at the load end of the distribution feeder,

$$V_s - V_r = \Delta V = \frac{RP_{net} + XQ_{net}}{V_r} \tag{10.10}$$

where $P_{net} = P_L - P_G \quad Q_{net} = Q_L - Q_G$.

Therefore, if P_{net} is negative ($P_G > P_L$), then the distribution feeder voltage will increase and voltage limits may be violated at the end of the feeder.

Example *A 20-km-long 11-kV distribution feeder provides power to a 450 kW, 140 kVA load. The distribution feeder has 0.3 Ω/km resistance and 0.031 Ω/km reactance. A 750 kVA distributed generator is installed at the load end of the feeder. Calculate the voltage rise in the feeder when it generates 650 kW active*

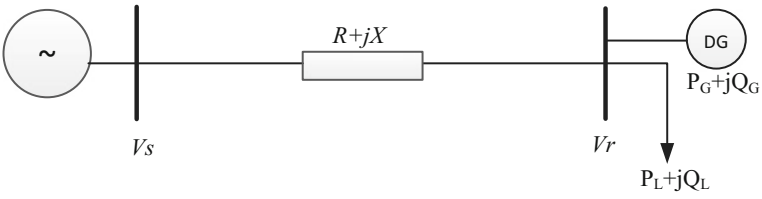

Fig. 10.13 Distribution feeder with a distributed generator

power at 0.9 leading power factor. Assume that the receiving-end voltage is 11 kV when the distributed generator is connected to the network.

$$\text{Voltage Rise}\,(\Delta V) = \frac{RP_{\text{net}} + XQ_{\text{net}}}{V_{\text{r}}}$$

$$\Delta V = \frac{(0.3 \times 20).(450 - 650) \times 10^3 + (0.031 \times 20).(140 - 314.81) \times 10^3}{11 \times 10^3}$$

$$\Delta V = -119\ V$$

The distribution feeder voltage will, therefore, increase by 119 V due to DG.

10.4.1 Voltage Rise Issues with Solar-PV Generation

In order to demonstrate the potential for voltage rise in distribution feeders with solar-PV generation, a simulation was carried out in DIgSILENT Power Factory for a LV distribution feeder (see Fig. 10.16). The LV distribution feeder was modelled with three separate single-phase feeder segments, and each phase contains 8 domestic households separated by 43.05 m. The distribution line has an impedance of 0.315 + j0.259 Ω/km. Also, it is assumed that every household has a 3.3 kVA solar-PV system. The simulation scenarios are shown in Table 10.3.

Figure 10.14 illustrates the voltage profiles observed for phase A of the distribution feeder for all three scenarios.

As illustrated in Fig. 10.14, for scenario 1 (midday scenario) voltage limits have not been violated at any of the distribution feeder nodes. However, the lower voltage limit has been violated by scenario 2 due to the high-load demand of the domestic households during the evening peak. Therefore, distribution transformer tap position is raised to an upper value (optimised position) in order to maintain the feeder voltage within stipulated voltage limits at all conditions, and this is depicted in scenario 3. It must be noted that the optimised tap position for scenarios 3 and 4 is position 4, and the additional voltage per tap is 2.5%. According to Fig. 10.14, in scenario 3, the feeder voltage is now maintained within the stipulated voltage limits at all nodes of the distribution feeder. As the distribution transformers are typically fixed-tap transformers, this will be fixed for an entire season. Therefore, when solar-PV is added to the network, it is likely that the feeder voltage increases

Table 10.3 Solar-PV scenarios for each household

Scenario	Load	Solar-PV	Description
1	2.4 kW, 0.95 pf lag	0	Midday, zero tap
2	12 kW, 095 pf lag	0	Evening peak, zero tap
3	12 kW, 095 pf lag	0	Evening peak, optimised tap
4	2.4 kW, 0.95 pf lag	3 kW	Midday with solar, optimised tap

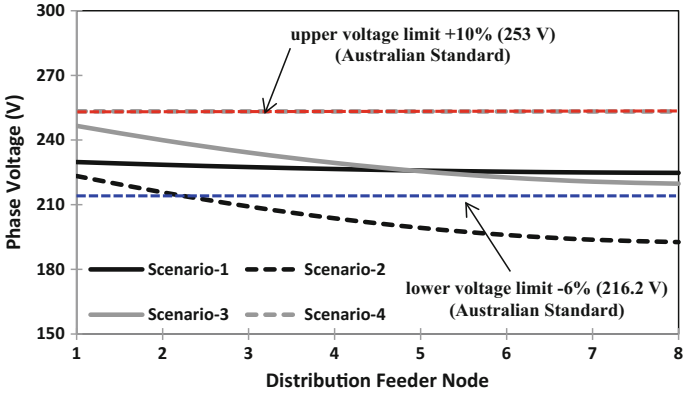

Fig. 10.14 Distribution feeder voltage variation

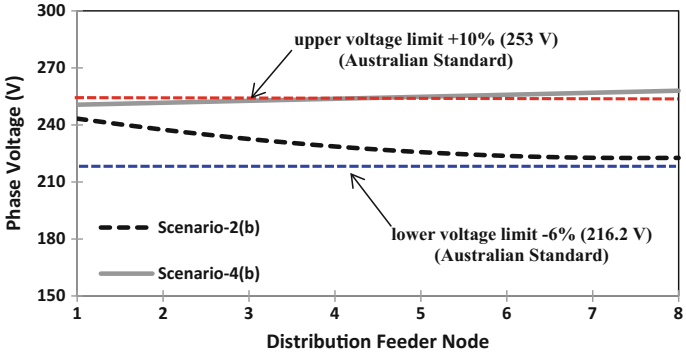

Fig. 10.15 Distribution feeder voltage variation with capacitor banks

beyond stipulated limits during low-load, midday conditions. This is evident from scenario 4 which depicts voltage increase due to the solar-PV generation.

Furthermore, it must be noted that increasing the tap position to improve the network voltage profile during high-load conditions would not be effective for long-distribution feeders as it may excessively increase the voltage at the start of the feeder. Therefore, for long-distribution feeders, capacitor banks are employed at the middle or near end of the distribution feeders in order to improve the voltage profile during high-load conditions, while maintaining the tap position at a low value. In order to demonstrate the deployment of capacitor banks in distribution feeders, an additional scenario was simulated considering load generation data given for scenario 2 and scenario 4 in Table 10.3. It is noted that the tap position is maintained at 3, while a capacitor bank rated at 20 kVAr per phase is now connected to the end of the feeder. Distribution feeder voltage profiles are shown in Fig. 10.15.

According to Fig. 10.15, when both the transformer tap operation and capacitor banks are used at the distribution feeder (scenario 2(b)), a much flatter voltage profile can be achieved in comparison with an optimised transformer tap position (scenario 2). For example, when an optimised transformer tap position is used, the distribution feeder voltage varies from 246.6 to 219.7 V, while for scenario 2(b) where both transformer tap operation and capacitor banks are used, the distribution feeder voltage profile varies only between 243 and 223 V. However, once the solar-PV generation is added to the distribution feeder (scenario 4(b)) with the same configuration (i.e. with fixed-transformer tap and capacitor banks), the distribution feeder voltage profile violates the stipulated limits at a much higher magnitude than scenario 4. Thus, voltage rise issue becomes much aggravated with solar-PV generation when transformer taps and capacitor banks are used in distribution feeders.

10.4.2 Voltage Regulation Methods with Distributed Solar-PV Generation

In order to mitigate the voltage rise in distribution feeders with solar-PV generation, the following methods are proposed by researchers, some of which are already applied to power distribution networks:

- Reactive power compensation by solar-PV inverter [3, 14],
- Energy storage systems (ESSs) [15], and
- Electronic tap-changing transformers [3].

- Reactive Power Compensation by solar-PV inverter.

As shown in Fig. 10.4, a solar-PV inverter has considerable reactive power capability, and that could be used to improve the voltage profile of the distribution feeder. Theoretically, reactive power compensation through solar-PV generation can be explained as follows:

Let us assume that both the sending-end voltage (V_s) and receiving-end voltage (V_r) are maintained at the same value by reactive power compensation at the receiving end of the feeder. Then, the voltage drop of the feeder becomes zero ($\Delta V = 0$). Therefore, Eq. (10.10) becomes:

$$\Delta V = \frac{RP_{\text{net}} + XQ_{\text{net}}}{V_r} = 0 \Rightarrow Q_{\text{net}} = -\frac{RP_{\text{net}}}{X} \tag{10.11}$$

Thus, in order to compensate for the voltage variation due to the change in P_{net}, Q_{net} must be maintained at $(-RP_{\text{net}}/X)$. Hence, the distributed generator must provide reactive power given by Eq. (10.12):

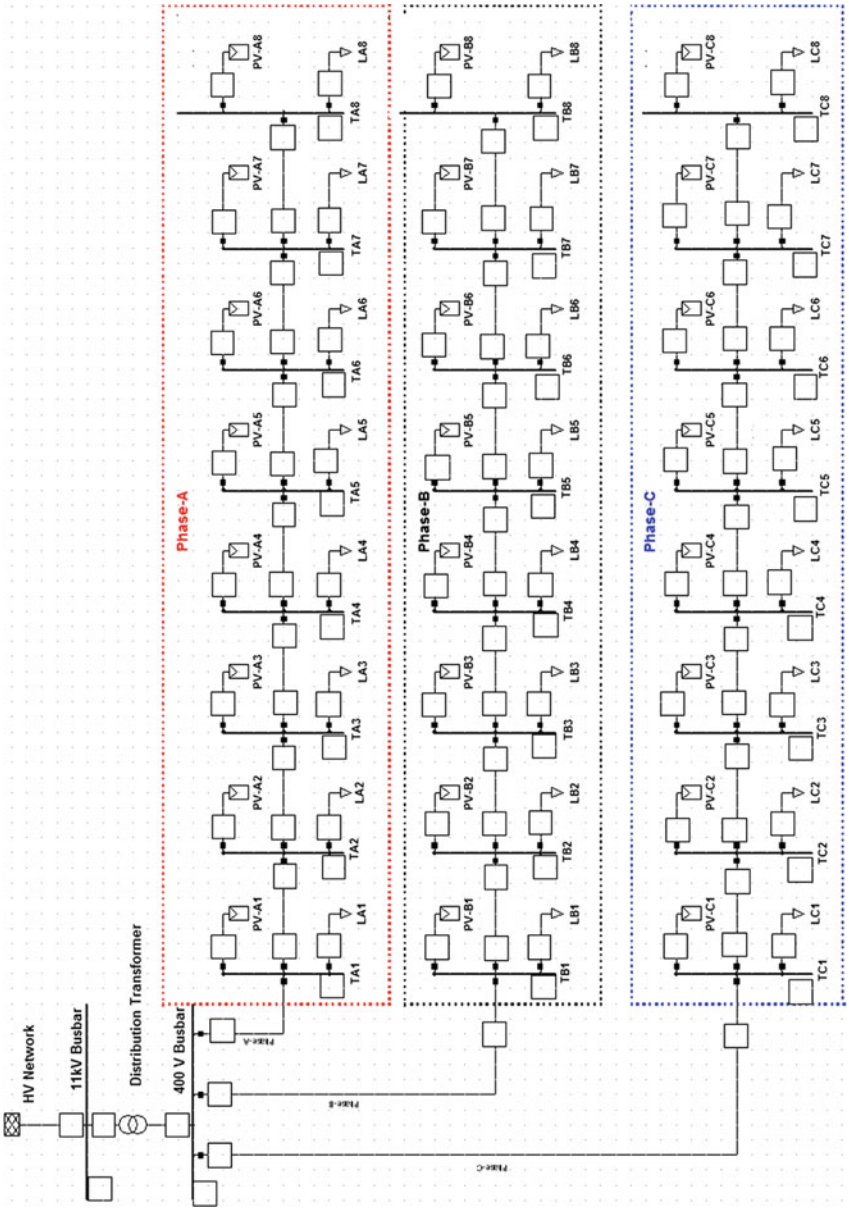

Fig. 10.16 Distribution feeder model

$$Q_{\mathrm{G}} = \frac{RP_{\mathrm{net}}}{X} + Q_{\mathrm{L}} \tag{10.12}$$

Based on the installed load in the distribution feeder and generation level of the solar-PV generator, the actual reactive power capability available from the solar-PV generation would be insufficient to mitigate the voltage increase in the distribution feeder; hence, some other methods must be used for distribution feeder voltage management.

- Energy Storage Systems

Energy storage systems (ESSs) can be used to overcome the voltage rise in distribution feeders. ESSs can be installed either at an individual household as single-phase units, or at a large scale as three-phase units on the distribution network. A schematic of an ESS is shown in Fig. 10.17.

ESSs are typically comprised of a VSI, line filter, coupling transformer, DC link and DC-DC converter, and energy source. Different types of energy sources are used, and this includes battery banks (e.g. Li-Ion), flywheels, supercapacitors, and superconducting magnetic storage. ESSs are capable of both delivering and absorbing active and reactive power to maintain the voltage at a given or set value.

- Electronic Tap-changing Transformers

Conventional distribution transformers are fixed-tap transformers; hence, tap positions are set manually, once every season. Therefore, distribution utilities do not have any control over tap position; thus, the control capability of the feeder voltage is fixed. Electronic tap-changing transformers offer flexibility at low cost in comparison with mechanical on-load tap-changing transformers. In electronic units, tap changing is performed by semiconductor switches, using either back-to-back thyristors or insulated gate bipolar transistors (IGBTs) [16]. The ability to move from one tap to any other tap repeatedly at half-cycle intervals enables high-speed voltage regulation in the distribution feeder, while it also helps manage the distribution feeder voltage profile with installed solar-PV generation to overcome cloud cover effects [3].

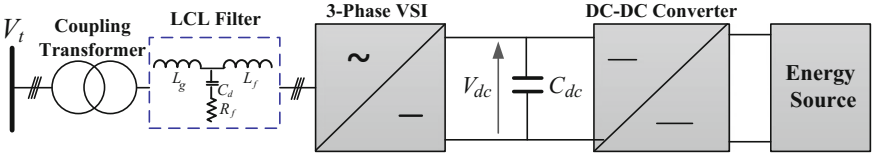

Fig. 10.17 Schematic diagram of an energy storage system

10.4.3 Case Study—Mitigation of Voltage Rise in Distribution Feeders with Solar-PV Generation

This section presents a case study to demonstrate the methods used for distribution feeder voltage regulation with installed solar-PV generation. The network presented in Fig. 10.16 and scenario 4 (presented in Table 10.3) has been used to demonstrate the capability of voltage regulation. In fact, two voltage regulation methods have been investigated separately: (i) solar-PV inverter reactive power capability (each solar-PV inverter absorbs 1.4 kVAr) and (ii) 50 kVA ESS installed at the end of the feeder. The ESS is configured to maintain the voltage at the end of the feeder at a predefined value. It is noted that the simulation was completed with the tap position set at 2 (2.5% change in each tap) and a 20 kVAr capacitor bank at each phase of the distribution feeder.

From Fig. 10.18, it is apparent that the distribution feeder voltage profile has substantially improved by using the reactive power capability of the inverter. It is also noted that 1.4 kVAr is the maximum reactive power output of the solar-PV inverter as it generates 3 kW (inverter rating 3.3 kVA). However, this reactive power capability is insufficient to maintain voltage levels below the stipulated maximum limit (in the Australian standard) at all nodes in the distribution feeder. Therefore, after node 6, the distribution feeder voltage exceeds stipulated limits. However, by employing a 50 kVA ESS, the distribution feeder voltage profile is maintained within stipulated limits.

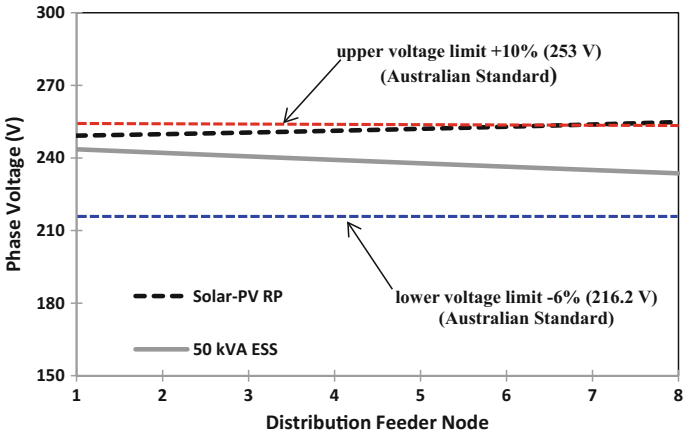

Fig. 10.18 Voltage regulation techniques with solar-PV generation

10.5 Voltage Stability with Solar-PV Generation

10.5.1 Voltage Stability Definition

Voltage stability is defined as the ability of a power network to maintain steady-state voltage levels across all nodes of the power network following a contingency in the network [17]. Voltage stability is strongly correlated with network reactive power capability, and conventional synchronous generators contribute significantly to network reactive power reserve. When renewable power penetration levels increase, synchronous generation is withdrawn from the energy portfolio; hence, reactive power reserves decrease as the renewable sources are incapable of providing the equivalent level of necessary reactive power reserve. If a significant solar-PV generation is installed in the distribution grid, the reactive power capability is limited due to inverter constraints and by the distribution transformer installed upstream of the distribution feeder [3].

Voltage stability can be evaluated using dynamic and static methods. In dynamic methods, a credible contingency is created in the network, and subsequently, voltage profiles are evaluated in the time domain to verify the network capacity to recover from a voltage dip created during the contingency [18]. Static voltage stability methods are developed based on load flow analysis, and commonly used static methods are P-V curve, Q-V curve, and modal analysis [18]. P–V curve analysis is mainly used to evaluate the impact of network load increase on voltage instability. The Q-V curve was used in previous studies to evaluate the voltage stability with renewable power generation as the renewable power generators are more likely to affect the reactive power reserve of the system [19]. Since distributed solar-PV generation also affects the network reactive power reserves, Q-V curve analysis is used in this chapter to evaluate the static voltage stability of the network.

The Q-V curve is generated by varying the reactive power at a given busbar and then determining the voltage at the same busbar by solving load flow for the network. Therefore, the Q-V curve method determines busbar voltage sensitivity to reactive power. Figure 10.19 illustrates the Q-V curve for a network busbar.

At steady state, the busbar voltage is maintained at Vss, while the reactive power at the steady state is Qss. When the reactive power is progressively increased, the bus voltage will decrease progressively until it reaches $dQ/dV = 0$. After this point, busbar voltage will further decrease even though the reactive power is decreased further.

10.5.2 Static Voltage Stability with Solar-PV Generation

The static voltage stability with solar-PV generation is evaluated using Q-V curve analysis for the model IEEE-14 bus network with solar-PV generation added to the LV network of the IEEE model. It is noted that solar-PV generation is added to the

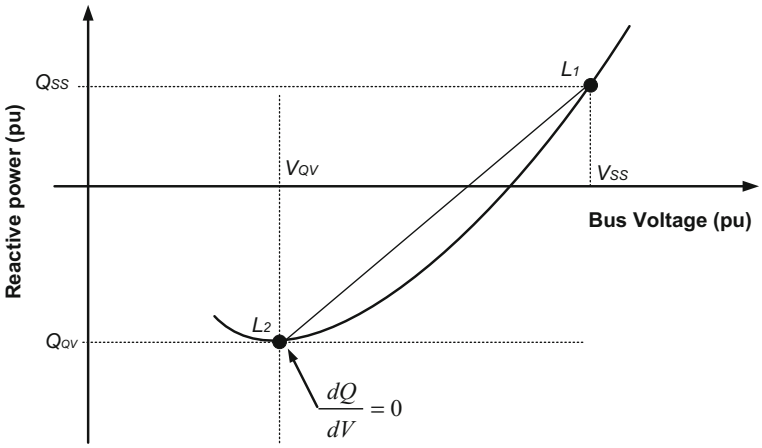

Fig. 10.19 Q-V curve method

Table 10.4 Generation portfolio for solar-PV scenarios

Scenario	Active power dispatch (MW)					
	Bus 1 (SG)	Bus 2 (SG)	Bus 11 (solar-PV)	Bus 12 (solar-PV)	Bus 13 (solar-PV)	Bus 14 (solar-PV)
1	232.9	40	0	0	0	0
2	210.2	40	5	5	5	5
3	188.0	20	15	15	15	15
4	168.3	0	25	25	25	25
5	128.1	0	35	35	35	35

network as aggregated three-phase solar-PV units, and synchronous generators are progressively withdrawn from the generation mix as the solar-PV levels increase. Solar-PV generation was added to buses 11, 12, 13, and 14, and solar-PV levels at each busbar were increased from 5 to 35 MW with 10 MW steps; subsequently, a Q-V curve was generated for each busbar. Also, note that the solar-PV generation was operated at unity power factor. The generation portfolio for each solar-PV scenario is shown in Table 10.4. It is noted that the synchronous machines at busbars 3, 6, and 8 are operated in synchronous condenser mode.

Figure 10.20 illustrates the V-Q curves generated for bus 3 and bus 12.

As illustrated in Fig. 10.21, integration of solar-PV generation with the distribution network rendered impacts in two ways. In terms of the high-voltage network, bus voltage stability decreased with solar-PV generation inclusion. For example, the voltage instability point reached −232 VAr consumption (with no solar-PV generation), while with a 140 MW solar-PV contribution (i.e. scenario 5) the instability point reached −181 VAr. Conversely, for the LV network, the V-Q instability point improved with the inclusion of solar-PV generation. Moreover, the voltage

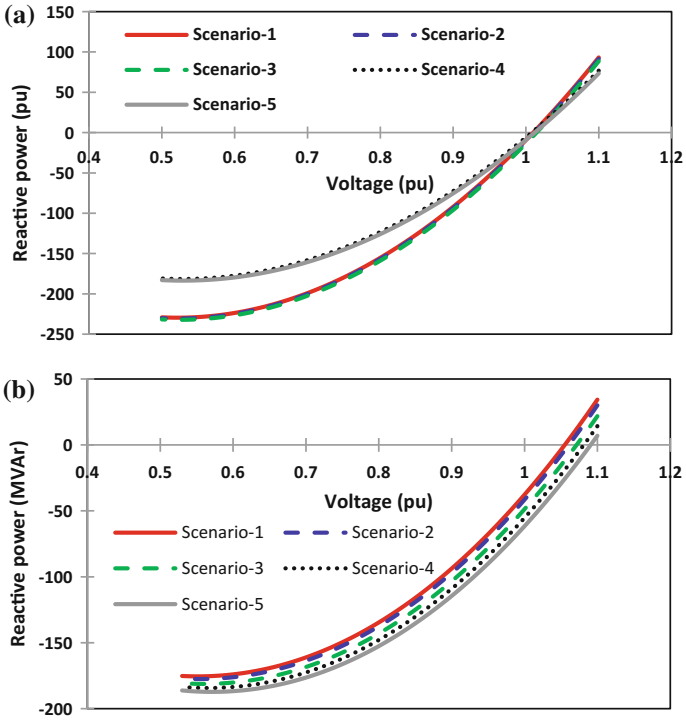

Fig. 10.20 V-Q curves: **a** bus 3 and **b** bus 12

instability point reached −177.5 VAr consumption (with no solar-PV generation), whereas with 140 MW solar-PV contribution, the instability point reached −187 VAr. Therefore, by integrating distributed solar-PV generation, the static voltage stability effectively improved in the HV network, while for the LV network, voltage stability deteriorated.

10.5.3 Dynamic Voltage Stability with Solar-PV Generation

The dynamic voltage stability was evaluated by creating a 150-ms three-phase, short-circuit fault at an HV node (bus 3) and on the LV network (bus 13). The scenarios 1 and 5 outlined in Table 10.4 have been analysed for dynamic voltage stability. For scenario 5, two additional scenarios were considered: (a) solar-PV with no dynamic voltage support and (b) solar-PV with dynamic voltage support. A dynamic three-phase solar-PV model outlined in [20] was used for simulations. The bus voltage variations following the short-circuit faults for scenarios 1 and 5 are shown in Fig. 10.22a and b, respectively.

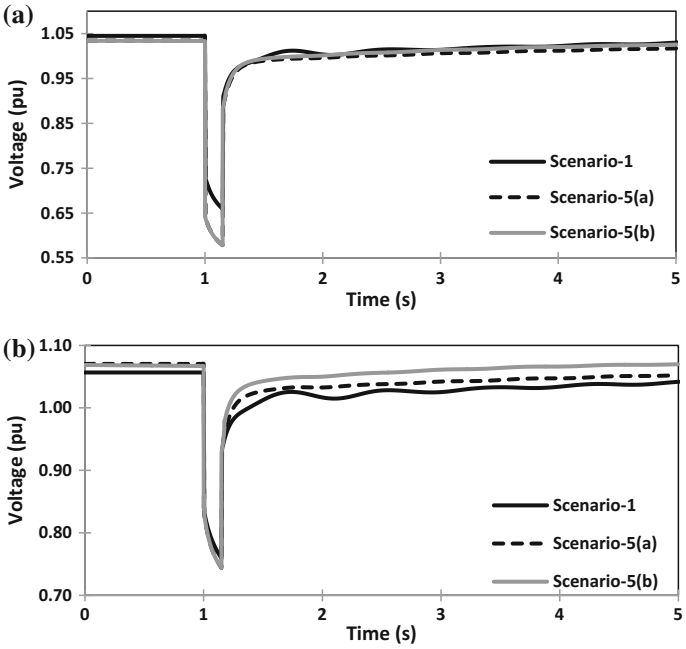

Fig. 10.21 Fault in the HV busbar (bus 3): **a** voltage variation at bus 2 and **b** voltage variation at bus 11

From Fig. 10.22, when a fault occurs at the HV busbar, it adversely affects the HV network for the scenario which includes solar-PV generation. Without solar-PV contribution, the HV network bus 2 voltage decreased to 0.65 pu, whereas with solar-PV inclusion, the bus voltage decreased to 0.56 pu. This occurred as a consequence of the removal of the conventional generation when the distributed solar-PV generation was added to the network. However, when the distributed generation is equipped with dynamic voltage support, this supports rapid HV bus voltage recovery—faster than with dynamic reactive power support.

In terms of the LV network buses, addition of distributed solar-PV generation significantly contributes to the recovery process of the LV bus voltage (i.e. bus 11) following the disturbance in the HV network. In particular, when the solar-PV generation is equipped with dynamic voltage support (scenario 5(b)), significant improvement in voltage recovery following the HV network fault is evident.

Similar observations are apparent when a fault occurs in the LV network (see Fig. 10.22), except that the LV network voltages decrease substantially compared to the HV network buses due to the close proximity to the fault.

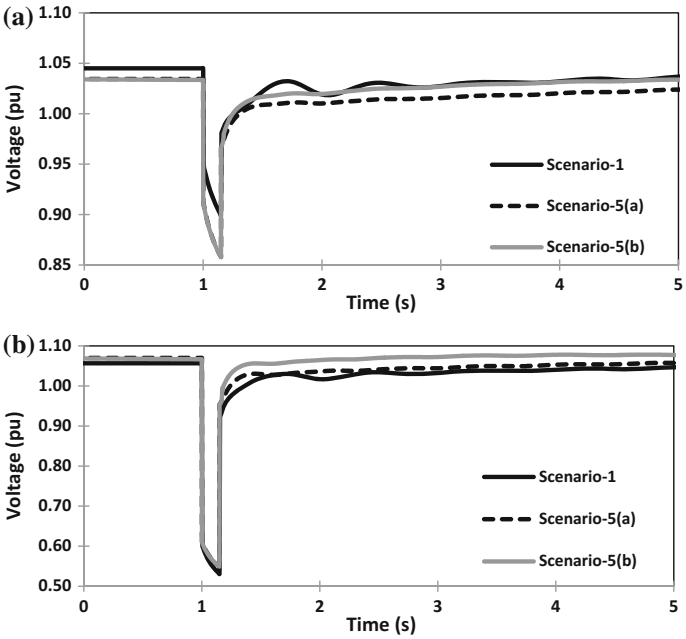

Fig. 10.22 Fault in the LV busbar (bus 13): **a** voltage variation at bus 2 and **b** voltage variation at bus 11

10.6 Discussion and Conclusions

This chapter has investigated feeder voltage control and voltage stability issues arising from high penetration of solar-PV generation in distribution networks. Voltage regulation methods have been investigated for conventional distribution feeders. This chapter has demonstrated that conventional voltage regulation approaches are broadly inadequate in managing distribution feeder voltage profiles when solar-PV generation is installed as voltage profiles can exceed stipulated limits imposed by relevant standards. Therefore, innovative methods that use power electronics technologies for voltage regulation, such as electronic tap-changing transformers, STATCOM, and ESS, have been presented to solve associated problems. This chapter has used several case studies to demonstrate the applicability of presented methods to manage distribution networks governed by stipulated standards and limits in voltage profile regulation. The results have further shown that multiple strategies may be required to regulate the feeder voltage profile under very high solar-PV penetration.

In addition, this chapter has investigated the impact of a high penetration of PV-solar generation on voltage stability using static and dynamic methods. The V-Q curve method, which analyses static voltage stability, demonstrates that solar-PV generation has an impact on HV and LV networks: as solar-PV generation

is added to an LV network, it adversely affects the voltage stability of the HV network, while the LV network benefits from improvements in voltage stability with the integration of solar-PV units. Furthermore, observations from dynamic voltage stability analyses indicate that while solar-PV generation can potentially weaken an HV network, integration can, however, strengthen LV distribution networks.

References

1. AEMO (2014) Renewable energy integration in South Australia. Available via http://www.aemo.com.au/Electricity/Planning/Integrating-Renewable-Energy. Accessed 4 Apr 2015
2. Fraunhofer ISE (2015) Recent facts about photovoltaics in Germany. Available via https://www.ise.fraunhofer.de/en/publications. Accessed 12 Mar 2015
3. Kabiri R, Holmes G, McGrath B, Meegahapola L (2015) LV grid voltage regulation using transformer electronic tap changing, with PV inverter reactive power injection. IEEE J Emerg Sel Top Power Electron 3(4):1182–1192
4. REC Peak Energy Series (2015) High performance solar modules. Available via http://www.recgroup.com/en. Accessed 17 Dec 2015
5. Villalva MG, Gazoli JR, Filho ER (2009) Comprehensive approach to modelling and simulation of photovoltaic arrays. IEEE Trans Power Electron 24(5):1198–1208
6. Hussein KH, Mota I (1995) Maximum photovoltaic power tracking: An algorithm for rapidly changing atmospheric conditions. IEE Proc Gener Transm Distrib 142(1):59–64
7. Liserre M, Blaabjerg F, Hansen S (2005) Design and control of an LCL-filter-based three-phase active rectifier. IEEE Trans Ind Appl 41(5):1281–1291
8. Feng G, Ding L, Loh PC, Tang Y, Wang P (2009) Indirect dc-link voltage control of two-stage single-phase PV inverter. In: IEEE Energy Conversion Congress and Exposition (ECCE 2009), Sep 2009
9. Weedy BM, Cory BJ, Jenkins N, Ekanayake JB, Strbac G (2012) Electric power systems, 5th edn. Willey, London
10. Short TA (2005) Electric power distribution equipment and systems. CRC Press (Taylor and Francis), New York
11. Siemens (2008) JFR-instruction-manual. Available via: http://www.energy.siemens.com/us/pool/us/power-distribution/voltage-regulators. Accessed 2 Apr 2016
12. Kundur P (2014) Power system stability and control. McGraw-Hill, New York
13. Steffel SJ, Caroselli PR, Dinkel AM, Liu JQ, Sackey RN, Vadhar NR (2012) Integrating solar generation on the electric distribution grid. IEEE Trans Smart Grid 3(2):878–886
14. Alam MJE, Muttaqi KM, Sutanto D (2015) A Multi-mode control strategy for VAr support by solar PV inverters in distribution networks. IEEE Trans Power Syst 30(3):1316–1326
15. Alam MJE, Muttaqi KM, Sutanto D (2012) Distributed energy storage for mitigation of voltage-rise impact caused by rooftop solar PV. In: IEEE Power and Energy Society General Meeting, San Diego, CA, USA
16. Faiz J, Siahkolah B (2011) Electronic tap-changer for distribution transformers. Springer, Charm, Switzerland
17. Kundur P et al (2004) Definition and classification of power system stability IEEE/CIGRE joint task force on stability terms and definitions. IEEE Trans Power Syst 19(3):1387–1401
18. Cutsem TV, Vournas C (1998) Voltage stability of electric power systems. Springer, Switzerland

19. Amarasekara HWKM, Meegahapola L, Agalgaonkar AP, Perera S (2013) Impact of renewable power integration on VQ stability margin. In: Power Engineering Conference (AUPEC). Hobart, Tasmania
20. Meegahapola L, Robinson D (2016) Dynamic modelling, simulation and control of a commercial building microgrid In: Smart Power Systems and Renewable Energy Systems Integration, Springer, Cham, Switzerland